Page 1 of 23. © Royal Aeronautical Society YYYY
doi: 10.1017/aer.2016.1

Verification & Validation of Lifting Line α- and Γ-Formulations for 3-D Planforms under Viscous Flows

Jose R. Chreim
jchreim@caltech.edu

Institute for Technological Research, Energy Infrastructure Laboratory, São Paulo, Brazil
University of São Paulo, Polytechnic School, São Paulo, Brazil
California Institute of Technology, Department of Mechanical and Civil Engineering, Pasadena, The United States of America

Joao L. D. Dantas

Institute for Technological Research, Energy Infrastructure Laboratory, São Paulo, Brazil
University of Strathclyde, Department of Naval Architecture, Ocean, and Marine Engineering, Glasgow, The United Kingdom

Karl P. Burr

Federal University of ABC, Center for Engineering, Modelling, and Applied Social Sciences, Santo André, Brazil

Gustavo R. S. Assi and C. Marcos M. Pimenta

University of São Paulo, Polytechnic School, São Paulo, Brazil

Received DD MM YYYY; revised DD MM YYYY; accepted DD MM YYYY.

ABSTRACT

Many adaptations of the Lifting-Line Theory have been developed since its conception to aid in preliminary aerodynamic wing design, but they typically fall into two main formulations, named α- and Γ-formulation, which differ in terms of the control points chordwise location and the variable updated during the iterative scheme. This paper assess the advantages and drawbacks of both formulations through the implementation of the respective methods and assessment through standard Verification & Validation procedures. Verification showed that the Γ-method poorly converges for wings with nonstraight quarter-chord lines, while the α-method presents adequate convergence rates and uncertainties for all geometries; it also showed that the Γ-method agrees most with analytic results from the Classic Lifting-Line Theory, indicating that it tends to overpredict wing lift. Validation and comparison to other modern Lifting-Line methods was done for similar geometries, and not only corroborated the poor converge and lift overprediction of the Γ-method, but also showed that the α-method presented the closest results to experimental data for almost all cases tested, concluding that this formulation is typically superior regardless of the wing geometry; these results indicate that the implemented α-method has a greater potential for the extension of the Lifting-Line Theory to more geometrically complex lifting surfaces other than fixed wings with straight quarter-chord lines and wakes constrained to the planform plane.

NOMENCLATURE

A	Constant of the function obtained with the Richardson Extrapolation
AR	Aspect Ratio
b	Wing span
c	Airfoil chord/wing chord at a given spanwise location
$\bar{c}$	Mean aerodynamic chord
C_d	Airfoil drag coefficient
C_D	Wing drag coefficient
C_l	Airfoil lift coefficient
C_L	Wing lift coefficient
ϵ_{C_L}	Absolute error for the wing lift coefficient
$\mathbf{F}$	Aerodynamic Force
h	Representative grid size
$\mathbb{J}$	Jacobian matrix
$\mathbf{l}$	Bound vortex length vector
$\mathbb{M}$	Influence matrix
M_{ij}	Influence matrix ij^{th} element
N	Number of horseshoe vortices / Control Points
p	Order of convergence of the Richardson Extrapolation
$\mathbf{r}$	Vector connecting the edge of the horseshoe vortex to a point in space
R	Array of residues
Re	Reynolds number
S	Planform area
$\mathbf{u}_n$	Airfoil normal unit vector
U_h	Grid numerical uncertainty
$\mathbf{v}$	Unit velocity vector

$\mathbf{V}$	Velocity vector
W	Normal velocity component
y	Spanwise direction

Greek Symbol

α	Angle of attack
δ	Relative to section
Δ	Variation
Γ	Circulation
Ω	Relaxation factor
ρ	Density
θ	Geometric twist / Zero lift angle of attack

Subscripts and Superscripts

∞	Free-stream
BV	Bound Vortex
CLL	Classical Lifting-Line
CP	Control Point
eff	Effective
HSV	Horseshoe Vortex
i,j	Pertaining to i^{th}/j^{th} section
k	Referring to the Horseshoe Vortex k^{th} edge
L0	Zero-lift
n	n^{th} time-step
rot	Rotation
TV	Trailing Vortex
Vis	Real airfoil data
ws	Wing section

1.0 Introduction

Wing Aerodynamic Design is one of the most benefited fields from the later development of *Computational Fluid Dynamics* (CFD), here referring to schemes that solve the Navier-Stokes equations through either *finite volumes*, *finite elements*, *finite differences*, or *spectral* methods, due to their accuracy for flows ranging from low[(1)] to high[(2)] Reynolds numbers; however, they currently present a drawback in computational cost as a full simulation ranges from hours to days in modern supercomputers. This bottleneck limits the application of CFD during early design phases as many flow and geometric features must be assessed, so its use is more convenient when higher resolution is needed.

Modern *Lifting-Line* (LL) methods, on the other hand, have a balance between cost and accuracy that make them attractive for early design, as it is possible to evaluate many wing and flow configurations at a much lower cost while retaining adequate fidelity. This characteristic broadened application to lifting surfaces other than wings, such as kites[(3)], hydrofoils[(4)], wind

turbines[5], and marine propellers[6] to name a few. Even time-dependent flows[7,8] and LL-CFD coupling[9,10,11] has been shown to be advantageous due to the significantly reduced computational cost yet relatively high flow topological detail.

Li et al.[8] used airfoil data from CFD on an unsteady LL formulation to estimate wing aerodynamic forces in preliminary design phase, obtaining good agreement with full 3-D unsteady CFD calculations in less than a tenth of the time. Likewise, Şugar-Gabor and Koreanschi[12] integrated a modern LL formulation into a simultaneous analysis and design methodology and showed that good accuracy was achieved at relatively low computational time, making it appropriate for conceptual-level design and optimization of lifting geometries.

Modern LL methods have been mainly divided into two formulations: α-formulations, which iteratively solve the system of nonlinear equations through changes in the *effective* Angle of Attack (AoA) α_{eff}, and a Γ-formulations, which do so through changes in the circulation distribution Γ. But the maturing of numerical methods for practical applications ultimately make them subject to quality and reliability assessment, and Verification & Validation (V&V) is one of the most used procedures for such purpose. While Verification is a mathematical exercise which shows that the modeled equations are solved correctly, Validation is a science/engineering activity which shows that what is being solved are the correct model equations[13], so V&V is a crucial procedure to the development and improvement of any numerical methods.

Therefore, this paper summarises implementations of α- and Γ-methods for wings and contrasts them through standard V&V procedures[14,13,15] for a series of geometries of interest. They are also compared against other implementations in the literature, which are different flavors of either formulations or a combination of the two. Results showed that, for most planforms tested, the Γ-method tends to overpredict wing lift in comparison to experiments, while the α-method typically has better convergence stability and overall agreement with experimental data.

2.0 The α and Γ Lifting-Line Theory of Wings

The original LL theory was crucial to the advance of modern aerodynamics[16,17] and the need for wings with arbitrary geometries at optimum aerodynamic efficiency motivated its improvement; Weissinger's Lifting-Line[18], for example, extended the theory to wings with nonstraight quarter-chord $\frac{c}{4}$ lines by forcing each discretised section to satisfy *Pistolesi's Boundary Condition*[19] (PBC) at the third quarter chord location $\frac{3c}{4}$, and inclusion of real airfoil data through iterative schemes date back to at least the 1950s[20].

Mainly two LL formulations arose from these improvements[21,8], and slightly different classification is used herein: (i) Γ-*formulations* refer to those whose *Bound Vortices* (BVs) and *Control Points* (CPs) are both placed over the $\frac{c}{4}$ line, as in Fig. 1, while the iterative scheme updates Γ, and (ii) α-*formulations* refer to those whose BV and CP are placed at $\frac{c}{4}$ and $\frac{3c}{4}$ lines respectively, as in Fig. 2, while the iterative scheme updates α_{eff}. According to such classification, there are also (iii) 'mixed'-formulations, referring to those whose BV-CP follow the α-formulation, but the iterative procedure follows the Γ-formulation[22], which eventually relaxes the PBC.

An acclaimed Γ-formulation was presented by Phillips & Snyder[23], who replaced the continuous *Horseshoe Vortex* (HSV) distribution by a finite number of discrete vortices in a *vortex-lattice* representation[17] and included real airfoil data through the knowledge of α_{eff}.

The obtained *airfoil lift coefficient* C_l would be compared against its potential estimates from a combination of the *Kutta–Joukowski Theorem* (KJT)[24] and its mathematical definition, and if the two differed, Γ would be iteratively updated through a Newton's scheme until they matched to a certain tolerance. Likewise, an example of α-formulation is presented in Chreim et al.[25], whose discretisation, C_l calculations, and convergence criterion are similar to the Γ-method, but with a different iterative scheme, as α_{eff} is recalculated[26] through changes in the chordwise CP locations[27,28], forcing Γ to be such that the induced velocities satisfy the PBC. In the next subsections, both formulations will be summarised.

2.1 The Γ-Method

For the sake of discussion on the differences between the two main LL formulations, a Γ-formulation (herein called Γ-method) originally proposed by Phillips & Snyder[23] is summarised in this subsection. Consider a wing and its wake represented by N HSVs, as in Fig. 1. The velocity $\mathbf{V}_{ij}^{HSV}$ induced at any i$^{\text{th}}$ CP in space by a j$^{\text{th}}$ HSV with circulation Γ_j is calculated by Eq. (1):

$$\mathbf{V}_{ij}^{HSV} = -\frac{\Gamma_j}{4\pi}\left[\frac{\mathbf{v}_\infty \times \mathbf{r}_{ij}^{(2)}}{r_{ij}^{(2)}(r_{ij}^{(2)} - \mathbf{v}_\infty \cdot \mathbf{r}_{ij}^{(2)})} - \frac{(r_{ij}^{(2)} + r_{ij}^{(3)})(\mathbf{r}_{ij}^{(2)} \times \mathbf{r}_{ij}^{(3)})}{r_{ij}^{(2)} r_{ij}^{(3)}(r_{ij}^{(2)} r_{ij}^{(3)} + \mathbf{r}_{ij}^{(2)} \cdot \mathbf{r}_{ij}^{(3)})} + \frac{\mathbf{r}_{ij}^{(3)} \times \mathbf{v}_\infty}{r_{ij}^{(3)}(r_{ij}^{(3)} - \mathbf{v}_\infty \cdot \mathbf{r}_{ij}^{(3)})}\right] \quad (1)$$

in which $\mathbf{r}_{ij}^{(k)} = \left(x_{cp,i} - x_{bv,j}^{(k)}, y_{cp,i} - y_{bv,j}^{(k)}, z_{cp,i} - z_{bv,j}^{(k)}\right)$ is the vector connecting the k$^{\text{th}}$ edge (for consistency with the α-method, $k = 2, 3$) of the j$^{\text{th}}$ BV, located at $\left(x_{bv,j}^{(k)}, y_{bv,j}^{(k)}, z_{bv,j}^{(k)}\right)$, to the i$^{\text{th}}$ CP, located at $\left(x_{cp,i}, y_{cp,i}, z_{cp,i}\right)$, and $\mathbf{v}_\infty$ is the free-stream unit velocity vector. The overall velocity $\mathbf{V}_i$ at this CP is the superposition of the free stream $\mathbf{V}_\infty$, the $N-1$ induced velocities from the other HSVs, and the induced velocities by i itself minus the BV component:

$$\mathbf{V}_i = \mathbf{V}_\infty - \frac{\Gamma_i}{4\pi}\left[\frac{\mathbf{v}_\infty \times \mathbf{r}_{ii}^{(2)}}{r_{ii}^{(2)}(r_{ii}^{(2)} - \mathbf{v}_\infty \cdot \mathbf{r}_{ii}^{(2)})} + \frac{\mathbf{r}_{ii}^{(3)} \times \mathbf{v}_\infty}{r_{ii}^{(3)}(r_{ii}^{(3)} - \mathbf{v}_\infty \cdot \mathbf{r}_{ii}^{(3)})}\right] + \sum_{j=1, j\neq i}^{N} \mathbf{V}_{ij}^{HSV} \quad (2)$$

The aerodynamic force $\delta\mathbf{F}_i$ normal to $\mathbf{V}_i$ and the BV length vector $\delta\mathbf{l}_i$ is obtained through the KJT:

$$\delta\mathbf{F}_i = \rho_\infty \Gamma_i \mathbf{V}_i \times \delta\mathbf{l}_i \quad (3)$$

with ρ_∞ the free-stream density. Likewise, its magnitude can be expressed through the definition of the section lift coefficient C_l:

$$\delta F_i = \frac{1}{2}\rho_\infty V_\infty^2 C_{l,i} \delta S_i \quad (4)$$

with δS_i the i$^{\text{th}}$ wing section area. Combining Eqs. (3) and (4):

$$C_{l,i} = 2\left(\frac{\Gamma_i}{\bar{c}_i V_\infty}\right)\left|\frac{\mathbf{V}_i}{V_\infty} \times \frac{\bar{c}_i \delta\mathbf{l}_i}{\delta S_i}\right| \quad (5)$$

in which $\bar{c}_i$ is a mean characteristic chord for purposes of nondimensionalization. Expression (5) is compared against real airfoil lift coefficient $C_{l,i}^{Vis}\left(\alpha_{eff,i}\right)$ from either experiments, simulations, or analytic/semi-empirical curves:

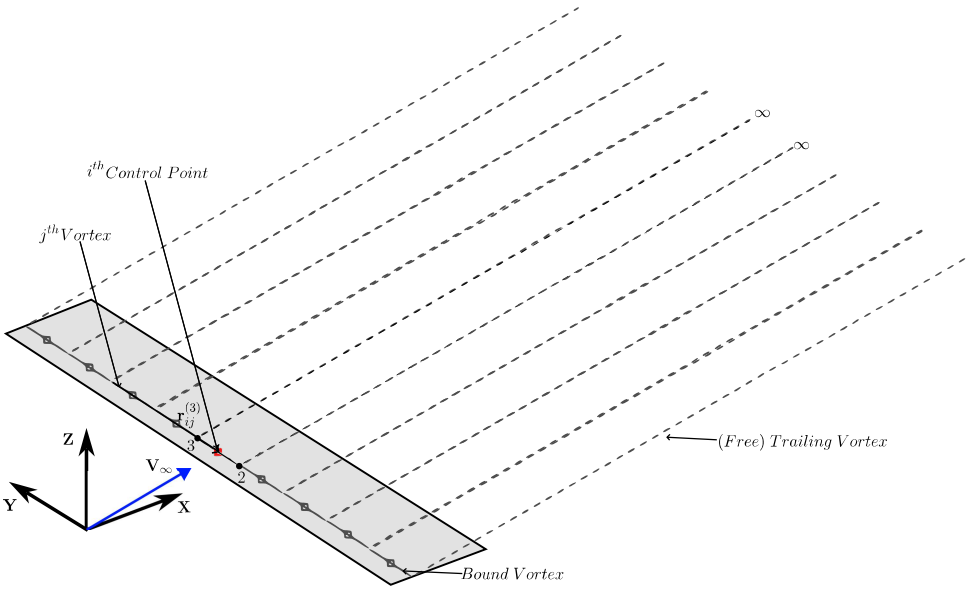

Figure 1. Horseshoe Vortex wing representation for the Γ-method

$$C_{l,i} - C_{l,i}^{Vis}\left(\alpha_{eff,i}\right) = R_i \tag{6}$$

with R_i the residue that is ideally 0 and $\alpha_{eff,i}$ calculated from $\mathbf{V}_i{}^{(23)}$. Equation (6) provides a system of N nonlinear equations that is iteratively solved for $\mathbf{\Gamma} \equiv (\Gamma_1, \Gamma_2, \cdots, \Gamma_N)$ and stops when $\mathbf{R} \equiv (R_1, R_2, \cdots, R_N) \approx \mathbf{0}$. With an adequate initial guess, from the linearised version of Eqs.(6), the method rapidly converges via Newton's method:

$$\mathbb{J}\left(\frac{\Delta\mathbf{\Gamma}}{\bar{\mathbf{c}}V_\infty}\right) = -\mathbf{R} \tag{7}$$

$$\mathbf{\Gamma^{n+1}} = \mathbf{\Gamma^n} + \Omega\bar{\mathbf{c}}V_\infty\left(\frac{\Delta\mathbf{\Gamma}}{\bar{\mathbf{c}}V_\infty}\right) \quad \Omega \in (0, 1] \tag{8}$$

with $\mathbb{J}$ the Jacobian matrix and Ω a subrelaxation factor (typically 0.8). The total aerodynamic forces, moments, and coefficients can be determined by numerically integrating Eq. (4), but the current discussion is limited to the *Lift* and *Drag* coefficients C_L and C_D. At this point, the *airfoil drag coefficient* $C_{d,i}$ can be included:

$$\begin{aligned} C_L &= \frac{1}{V_\infty^2 S}\sum_{i=1}^{N} V_i^2 \delta S_i \left[C_{l,i}\cos\left(\alpha_{rot,i}\right) - C_{d,i}\sin\left(\alpha_{rot,i}\right)\right] \\ C_D &= \frac{1}{V_\infty^2 S}\sum_{i=1}^{N} V_i^2 \delta S_i \left[C_{l,i}\sin\left(\alpha_{rot,i}\right) + C_{d,i}\cos\left(\alpha_{rot,i}\right)\right] \end{aligned} \tag{9}$$

in which α_{rot} refers to the rotation angle relating airfoil and wing coordinate systems, and includes the geometric twist, zero-lift, and induced angles. The Γ-method yields adequate

results for regions up to stall and planforms whose $\frac{c}{4}$ are straight; grid convergence analysis indicates, however, convergence issues for $\frac{c}{4}$ lines with sweep angles[29,30,31], so recent work[32,33] adapted the method to overcome this drawback.

2.2 The α-Method

Again, to highlight the differences between the two main formulations, an α-formulation (herein called α-method), proposed by Chreim et al.[25], is summarised in this subsection. The chosen HSV geometry is depicted in Fig. 2, and Eq. (1) is adjusted accordingly:

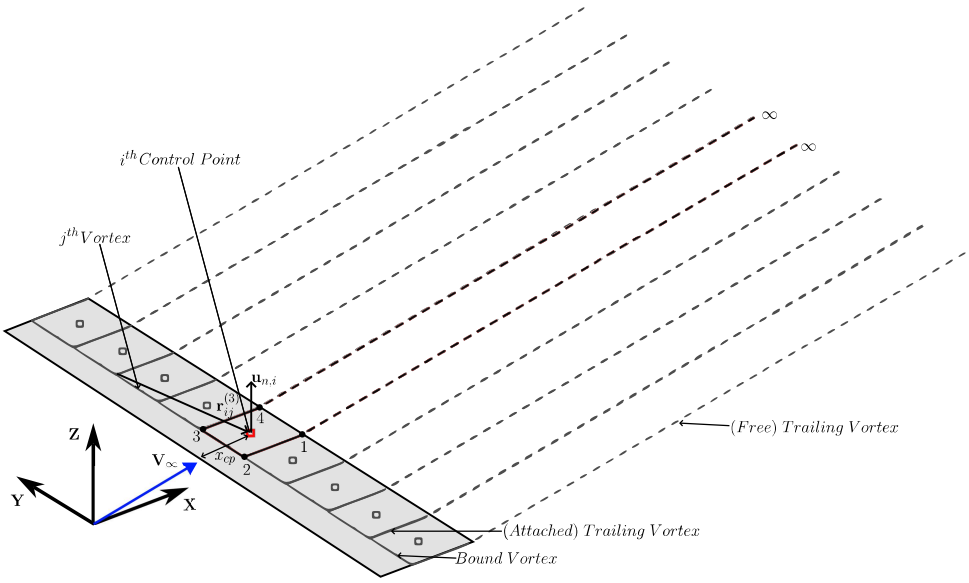

Figure 2. Horseshoe Vortex wing representation for the α-method

$$\mathbf{V}_{ij}^{HSV} = -\frac{\Gamma_j}{4\pi}\left[\frac{\mathbf{v}_\infty \times \mathbf{r}_{ij}^{(1)}}{r_{ij}^{(1)}(r_{ij}^{(1)} - \mathbf{v}_\infty \cdot \mathbf{r}_{ij}^{(1)})} - \frac{(r_{ij}^{(1)} + r_{ij}^{(2)})(\mathbf{r}_{ij}^{(1)} \times \mathbf{r}_{ij}^{(2)})}{r_{ij}^{(1)} r_{ij}^{(2)}(r_{ij}^{(1)} r_{ij}^{(2)} + \mathbf{r}_{ij}^{(1)} \cdot \mathbf{r}_{ij}^{(2)})}\right.$$
$$\left. - \frac{(r_{ij}^{(2)} + r_{ij}^{(3)})(\mathbf{r}_{ij}^{(2)} \times \mathbf{r}_{ij}^{(3)})}{r_{ij}^{(2)} r_{ij}^{(3)}(r_{ij}^{(2)} r_{ij}^{(3)} + \mathbf{r}_{ij}^{(2)} \cdot \mathbf{r}_{ij}^{(3)})} - \frac{(r_{ij}^{(3)} + r_{ij}^{(4)})(\mathbf{r}_{ij}^{(3)} \times \mathbf{r}_{ij}^{(4)})}{r_{ij}^{(3)} r_{ij}^{(4)}(r_{ij}^{(3)} r_{ij}^{(4)} + \mathbf{r}_{ij}^{(3)} \cdot \mathbf{r}_{ij}^{(4)})} + \frac{\mathbf{r}_{ij}^{(4)} \times \mathbf{v}_\infty}{r_{ij}^{(4)}(r_{ij}^{(4)} - \mathbf{v}_\infty \cdot \mathbf{r}_{ij}^{(4)})}\right] \tag{10}$$

Likewise, $\mathbf{V}_i$ now considers the contribution of all $5N$ segments:

$$\mathbf{V}_i = \mathbf{V}_\infty + \sum_{j=1}^{N} \mathbf{V}_{ij}^{HSV} \tag{11}$$

The α-method requires the enforcement of the PBC[19]:

$$\mathbf{u}_{n,i} \cdot \mathbf{V}_i = 0 \rightarrow \sum_{j=1}^{N} \mathbf{u}_{n,i} \cdot \mathbf{V}_{ij}^{HSV} = -\mathbf{u}_{n,i} \cdot \mathbf{V}_\infty \tag{12}$$

with $\mathbf{u}_{n,i}$ the i$^{\text{th}}$ normal unit vector; unlike the Γ-method, the α-method does not require a force equivalence, but rather a no-flux condition at the CPs[19], so Eq. (12) can be cast into a matrix form:

$$\mathbb{M}\boldsymbol{\Gamma} = -\mathbf{W}_\infty \tag{13}$$

with:

$$M_{ij} = \mathbf{u}_{n,i} \cdot \mathbf{V}_{ij}^{HSV}; \quad W_{\infty,i} = \mathbf{u}_{n,i} \cdot \mathbf{V}_\infty \tag{14}$$

Note that Eq. (13) is nonlinear as $\mathbb{M}$ depends on the CP locations, which depend on C_l^{Vis}, so $\boldsymbol{\Gamma}$ must be solved iteratively as follows: after a first estimate for $\boldsymbol{\Gamma}$, whose initial guess comes from assuming $x_{cp,i} = \frac{3}{4}c_i \ \forall i = 1, \cdots, N$ (implying $\frac{\partial C_{l,i}}{\partial \alpha_i} = 2\pi$) $C_{l,i}$ is calculated through Eq. (5), but with $\mathbf{V}_i$ and $\mathbf{V}_\infty$ replaced by the velocity $\mathbf{V}_i^{C_l}$ induced by only the *attached* and *free* trailing vortices[17] plus the free-stream:

$$\mathbf{V}_i^{C_l} = \mathbf{V}_\infty + \sum_{j=1}^{N} \mathbf{V}_{ij}^{TV} \tag{15}$$

$$\mathbf{V}_{ij}^{TV} = -\frac{\Gamma_j}{4\pi}\left[\frac{\mathbf{v}_\infty \times \mathbf{r}_{ij}^{(1)}}{r_{ij}^{(1)}\left(r_{ij}^{(1)} - \mathbf{v}_\infty \cdot \mathbf{r}_{ij}^{(1)}\right)} - \frac{\left(r_{ij}^{(1)} + r_{ij}^{(2)}\right)\left(\mathbf{r}_{ij}^{(1)} \times \mathbf{r}_{ij}^{(2)}\right)}{r_{ij}^{(1)} r_{ij}^{(2)}\left(r_{ij}^{(1)} r_{ij}^{(2)} + \mathbf{r}_{ij}^{(1)} \cdot \mathbf{r}_{ij}^{(2)}\right)} - \frac{\left(r_{ij}^{(3)} + r_{ij}^{(4)}\right)\left(\mathbf{r}_{ij}^{(3)} \times \mathbf{r}_{ij}^{(4)}\right)}{r_{ij}^{(3)} r_{ij}^{(4)}\left(r_{ij}^{(3)} r_{ij}^{(4)} + \mathbf{r}_{ij}^{(3)} \cdot \mathbf{r}_{ij}^{(4)}\right)} + \frac{\mathbf{r}_{ij}^{(4)} \times \mathbf{v}_\infty}{r_{ij}^{(4)}\left(r_{ij}^{(4)} - \mathbf{v}_\infty \cdot \mathbf{r}_{ij}^{(4)}\right)}\right]$$

If $C_{l,i}$ differs from $C_{l,i}^{Vis}$, the i$^{\text{th}}$ CP location is adjusted, effectively changing $\mathbf{r}_{ij}^{(k)}$ and consequently $\mathbf{V}_i$ or, equivalently, $\alpha_{eff,i}$, as the slope of the $C_{l,i} \times \alpha$ curve $\frac{\partial C_{l,i}}{\partial \alpha_i}$ changes[17]. After, $\boldsymbol{\Gamma}$ is updated. Mathematically, this happens according to the procedure indicated on Tab. 1:

Table 1
Iterative solution procedure for the α-method

1.	$C_{l,i}^n$ from (5) with $\mathbf{V}_i^{C_l}$ in (15)
2.	$\alpha_{eff,i}^n \approx \frac{C_{l,i}^n - \cancelto{0}{C_{l,i}(\alpha_{L0,i})}}{\frac{\partial C_{l,i}^n}{\partial \alpha_i}} + \alpha_{L0,i} = \frac{C_{l,i}^n}{\frac{\partial C_{l,i}^n}{\partial \alpha_i}} + \alpha_{L0,i}$
3.	$\frac{\partial C_{l,i}^{Vis}}{\partial \alpha_i} \approx \frac{C_{l,i}^{Vis}\left(\alpha_{eff,i}^n\right) - \cancelto{0}{C_{l,i}^{Vis}(\alpha_{L0,i})}}{\alpha_{eff,i}^n - \alpha_{L0,i}} = \frac{C_{l,i}^{Vis}\left(\alpha_{eff,i}^n\right)}{\alpha_{eff,i}^n - \alpha_{L0,i}}$
4.	$\frac{\partial C_{l,i}^{n+1}}{\partial \alpha_i} = \frac{\partial C_{l,i}^n}{\partial \alpha_i} + \Omega\left(\frac{\partial C_{l,i}^{Vis}}{\partial \alpha_i} - \frac{\partial C_{l,i}^n}{\partial \alpha_i}\right) \quad \Omega \in (0, 1]$
5.	$x_{cp,i}^{n+1} = \left[\frac{1}{2}\frac{\frac{\partial C_{l,i}^{n+1}}{\partial \alpha_i}}{2\pi} + \frac{1}{4}\right] c_i$, $y_{cp,i}^{n+1}$ and $z_{cp,i}^{n+1}$ accordingly
6.	$\mathbf{r}_{ij}^{(k),n+1} = \left(x_{cp,i}^{n+1} - x_{bv,j}^{(k)}, y_{cp,i}^{n+1} - y_{bv,j}^{(k)}, z_{cp,i}^{n+1} - z_{bv,j}^{(k)}\right)$
7.	$\mathbf{V}_i^{n+1}$ from (10) and (11), $\boldsymbol{\Gamma}^{n+1}$ from (13)

in which Ω is again typically 0.8. Table 1 shows that the the viscous $C_l^{Vis} \times \alpha$ curve is approximated by a linear interpolation, while the potential $C_l \times \alpha$ curve is iteratively adjusted based on $C_l^{Vis} \times \alpha$. The iterative scheme is illustrated in Fig. 3, which stops when $\mathbf{R} \approx \mathbf{0}$. The aerodynamic coefficients are obtained through Eqs. (9).

As a final note, the vortex-lattice representation is advantageous as it easily enables the construction of wings with arbitrary shape as, contrary to formulations that approximate the

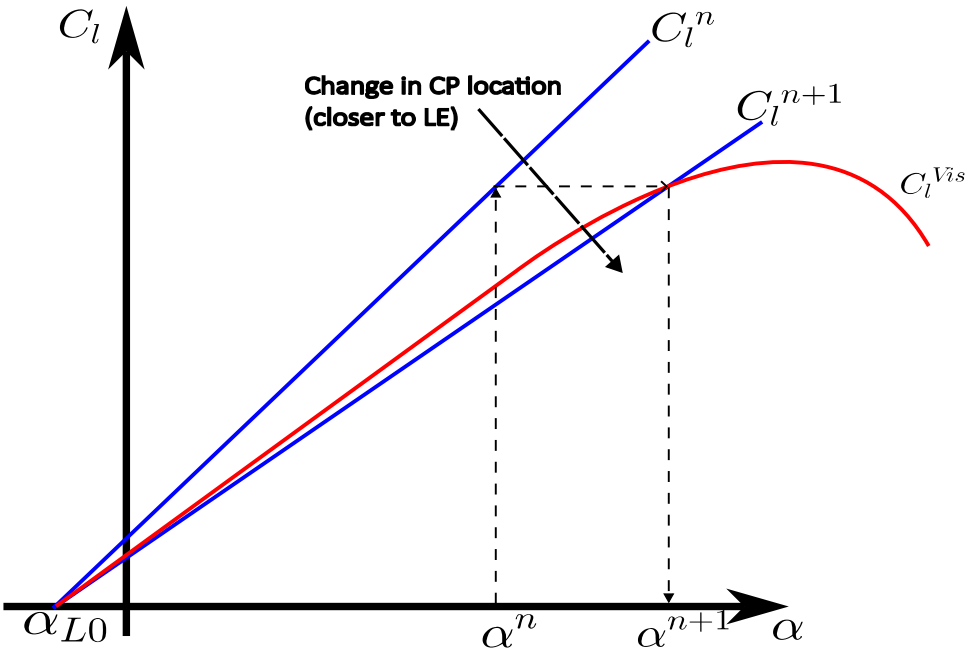

Figure 3. Illustrative example of the inclusion of real airfoil data on the α-method.

circulation distribution by a Fourier Series[26,21], no parametric curve or arclength is needed to generate the geometry but rather information about the wing chord length at a given spanwise location. Additionally, this representation requires the CP locations to change[34,28] rather than α_{eff} directly[26,21]; simply changing α_{eff} in this formulation would not adjust the $C_l \times \alpha$ curve slope[27], so the only possible solution would be $\alpha_{eff} = \alpha_{L0}$. It is also important to ensure that the CPs remain co-planar to the wing planform[31].

3.0 Results from Verification & Validation

In this section, both α- and Γ-methods prediction capabilities are assessed through standard Verification & Validation (V&V) procedures[15]; after error and uncertainty estimation, they are compared against experimental results and other implementations from the literature.

Verification, presented in section 3.1, is composed by Code and Solution Verification, intended to verify that a given code correctly solves the equations of the model and to estimate numerical error ϵ_ϕ and uncertainty U_N that arise from discretisation, iteration, and numerical precision. To this end, different planform geometries were assessed for grid convergence, and those with existing analytic solutions were further assessed to measure how much both methods deviate from the Classic Theory.

Validation, presented in section 3.2, aims to estimate the extent within which modeling error lies, accomplished by comparison with experimental data for a wide range of numerical testing conditions. Similar planform geometries were validated, and the methods were further compared to other state-of-the-art implementations.

The importance of V&V in the reliability of LL methods is illustrated by two examples. The

Γ-method was claimed capable of simulating lifting surfaces with arbitrary camber, sweep, and dihedral[23], which was later shown not to be the case for swept wings[30,31]. Changes in the locus of the BVs and in the geometry of the TVs circumvented the convergence issues, but these changes influence the final circulation distribution[30,33]. Likewise, literature showed good agreement of the α-method with experimental data including low Aspect-Ratio (AR) planforms[28], but the solutions were sensible to discretisation, and planform-dependent upper bounds for grid refinement were observed[28]. This issue was addressed by adapting the HSVs configuration[35], and preliminary Verification studies showed grid independence of the solution, but at the cost of restricting the method to moderate- and high-AR planforms. The remaining of this paper not only formally confirm previous results but also extend them to more general conclusions by means of standard V&V procedures.

3.1 Code and Solution Verification

Procedures for Code and Solution Verification and for error and uncertainty estimation are well reported in several references, and the approach taken follows the ASME Standard for Verification and Validation in CFD[15] and the work of Eça & Hoekstra[13]. Convergence was assessed by C_L, with the numerical uncertainty $U_N \equiv U_r + U_i + U_h$, made of round-off U_r, iterative U_i, and discretisation U_h uncertainties, assumed to be dominated by the discretisation uncertainty U_h; such assumption is reasonable as calculations were carried using double-precision arithmetic, ensuring round-off error to be about 10^{-16} while both iterative and discretisation error were at most in the order of 10^{-10}, significantly smaller than the orders of C_L; on the other hand, when convergence issues happened U_h was much higher than the other sources.

The methods were tested for planforms whose analytic solutions derived from the Classic Lifting-Line theory, so specific aspects of the implementations could be assessed. For *elliptically-loaded wings*, Prandtl's equation reduces to[36]:

$$\Gamma(y) = \Gamma(0)\left[1 - \left(\frac{2y}{b}\right)^2\right]^{1/2} = \frac{1}{2}\frac{\partial C_l}{\partial \alpha}\bigg|_y c(y)\left\{V_\infty\left[\alpha(y) + \theta(y)\right] - \frac{\Gamma(0)}{2b}\right\} \tag{16}$$

in which y refers to the wing spanwise direction and $\theta(y)$ spanwise twist and/or zero-lift angle. Equation (16) reveals many ways to geometrically generate elliptic lift distributions, so three planforms were generated and their characteristics were summarised on Tab. 2: (i) *Elliptical Planform* refers to a spanwise elliptical $c(y)$ distribution to test the methods capabilities in the presence of variable local incidence velocity and effective AoA; (ii) *Elliptical Slope* refers to a spanwise elliptical $\frac{\partial C_l}{\partial \alpha}(y)$ distribution to assess the inclusion of airfoil data that deviate from the ideal 2π rad^{-1}; and (iii) *Elliptical Twist* refers to a $\theta(y)$ distribution to test the methods capabilities for nonplanar wing geometries. Two additional configurations with no analytic solutions were also included: (iv) *Sweptback* refers to a 45-degree sweptback planform and (v) *Dihedral* refers to a 4-degree dihedral one. All these geometric properties are important not only to aerodynamic wing design, but also to the extension of LL methods to rotating lifting-surfaces[6].

The discretisation error ϵ_{C_L} was first estimated through a five-step procedure for the application of the Grid Convergence Index, based on a power-series representation, or *Richardson Extrapolation* Method (RE)[15]:

Table 2
Wings used for verification

Wing	Planform	$\frac{\partial C_l}{\partial \alpha}$ distribution	θ distribution
Elliptical Planform	Elliptical	2π	0
Elliptical Slope	Rectangular	Elliptical	0
Elliptical Twist	Rectangular	2π	Elliptical
Sweptback	Rectangular (45 deg sweepback)	2π	0
Dihedral	Rectangular (4 deg dihedral)	2π	0

$$\epsilon_{C_L} \simeq \delta_{RE} = C_L(h_j) - C_{Lext} = Ah_j^p + H.O.T, \quad h_j = \frac{\sum_{i=1}^{N_j} \delta l_i}{N_j} \tag{17}$$

with δ_{RE} the RE estimate, A a constant, p the observed order of grid convergence, h_j a typical grid size, and $C_{Lext} = \lim_{h_j \to 0} C_L\left(h_j\right)$. Equation (17) assumes that the solutions are in the *asymptotic range* to ensure high-order terms (H.O.T) can be neglected and that the grids could be represented by the single typical grid size h_j, which requires an almost constant grid refinement ratio $rr_j \equiv \frac{h_{j+1}}{h_j}$ and unaffected grid properties; while the former is virtually impossible to be determined[15,13], the latter is easily attainable for LL methods. Finally, cosine clustering discretisation was preferred, as convergence is expected to happen faster than equidistant clustering for the same family of grids[23,17].

The procedure was applied on several grid triplets, and if the attempt was not successful or if significantly discrepant results were found for the successive triples, i.e. significantly different p that arise from small data perturbations, then non-weighted (LSN) and weighted (LSW) least square approaches were applied at two extra sets[13], one from grids I to IV, and the other from I to V. The best approach was determined based on the least square that yielded the smallest standard deviation σ, given all data were classified as monotonically convergent ($p > 0$)[13]; when $p > 2.1$ or $p < 0.5$, however, δ_{RE} was dropped in favor of more appropriate estimators, δ_1, δ_2, or δ_{12}, that were again evaluated by LSN and LSW and the chosen estimator based on the smallest σ[13]:

$$\epsilon_{C_L} \simeq \delta_1 = A_1 h_j \tag{18}$$

$$\epsilon_{C_L} \simeq \delta_2 = A_2 h_j^2 \tag{19}$$

$$\epsilon_{C_L} \simeq \delta_{12} = A_1 h_j + A_2 h_j^2 \tag{20}$$

Note that the A_s in the expressions (18) to (20) are, in general, different. The same procedure was applied to estimate the uncertainty associated with C_D that will be used later in the $C_L \times C_D$ plots, although not reported in the paper. With Code and Solution Verification results established, analytic C_L from the elliptically-loaded planforms were compared to results from both methods by varying the AoA while keeping the geometry fixed and vice-versa. Results are presented next.

3.1.1 Convergence Analysis

For a fixed AoA of 4°, a set of 14 grids was simulated with $N_{max} = 7168$ (grid 'I'), $N_{min} = 80$ (grid 'XIV'), and $rr_j \approx \sqrt{2}$. Three subsets of three adjacent grids were used for estimation of ϵ_{C_L} through RE; however, as this procedure did not yield adequate results for almost all cases, the least square approach was preferred.

Figure 4 presents $(C_L(h) - C_{Lext}) \times \frac{h}{h_{min}}$ (dots) and $Ah^p \times \frac{h}{h_{min}}$ (lines) for all planforms; while for the elliptically-loaded wings, both methods perform equally well, for the Sweptback and Dihedral wings, the α-method significantly outperforms the Γ-method, whose plots indicate convergence issues.

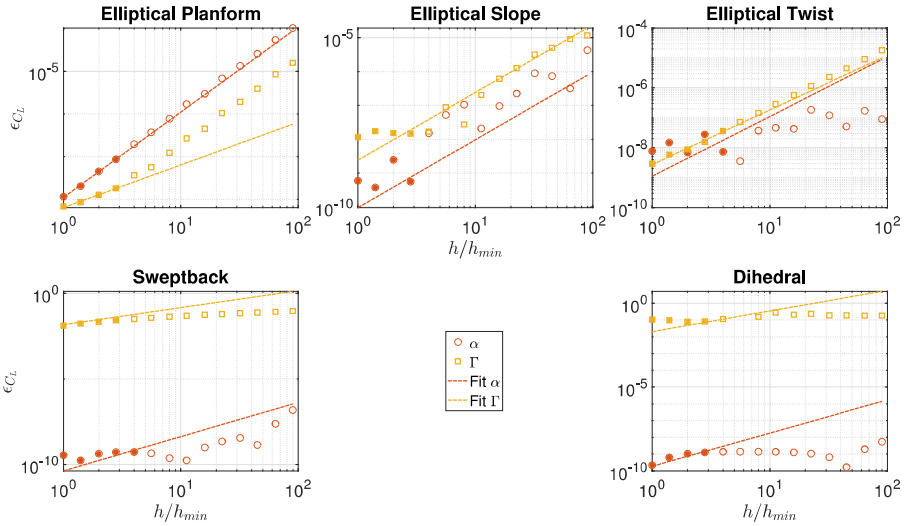

Figure 4. Convergence rates for the α- and Γ-methods.

The observed p and U_h, relative to C_{Lext}, are summarised in Tab. 3. For the α-method, $p \approx 2$ for almost all wings and even when more appropriate estimators are used, those are of quadratic order; the maximum U_h is not higher than 10^{-4}%. For the Γ-method, in the case of the elliptically-loaded wings most p and U_h are similar to the α-method, with the exception of p for the Elliptical Planform wing, whose best error estimator was of first order; for the Sweptback and Dihedral wings, the method presents convergence issues[15], which can be observed by the uncertainties ranging from 10^{+1}% to from 10^{+3}%. Therefore, these results formally extend what has been initially reported in the literature[31,32]: while Γ-formulations present convergence issues not only to planforms with sweep angles, but non-straight $\frac{c}{4}$ lines in general, α-formulations are naturally more advantageous for solving more complex geometry configurations.

LL Methods are designed to be computationally fast, and although the literature has suggested that grid convergence is obtained for $N \geqslant 80$[37,23], to the knowledge of the authors no uncertainty quantification has been reported. Therefore, the same analysis is performed for grids of *practical purposes* ($N_{max} = 224$), whose results are presented in Tab. 4; for the elliptically loaded wings both methods again returned p within acceptable ranges[13] and although U_h increased by up to 1000 times in a few cases, they are still negligible with respect

Table 3
Results for Grid Convergence. For $p < 0.5$ and $p > 2.1$, δ_{Re} was substituted for appropriate estimators - Finest grids ($N_{max} = 7168$)

Wing	Elliptical Planform		Elliptical Slope		Elliptical Twist		Sweptback		Dihedral	
Method	α	Γ	α	Γ	α	Γ	α	Γ	α	Γ
Grid Set	I to IV	I to IV	I to IV	I to IV	I to V	I to V	I to V	I to IV	I to IV	I to IV
Procedure	LSN	LSN	LSW	LSN	LSW	LSW	LSN	LSN	LSN	LSN
p	δ_2	δ_1	2.0	2.0	2.0	1.8	2.0	δ_{12}	2.0	1.2
σ	1.2E-9	4.3E-10	2.2E-9	2.0E-8	1.9E-8	1.7E-9	3.8E-10	1.8E-4	6.0E-10	1.6E-1
U_h (%)	4.7E-6	2.6E-6	7.2E-6	8.4E-5	5.6E-5	5.5E-7	1.6E-6	1.1E+1	1.0E-6	1.2E+3

to C_L and other sources of uncertainty. For the Sweptback and Dihedral wings, the results are almost the same as in the case of the most refined grids, with the associated uncertainties still large for the Γ-method. Therefore, $N = 224$ presents a good compromise between accuracy and computation time and so is used for the remaining of this paper.

Table 4
Results for Grid Convergence. For $p < 0.5$ and $p > 2.1$, δ_{Re} was substituted for appropriate estimators - 'Practical Purposes' grids ($N_{max} = 224$)

Wing	Elliptical Planform		Elliptical Slope		Elliptical Twist		Sweptback		Dihedral	
Method	α	Γ	α	Γ	α	Γ	α	Γ	α	Γ
Grid Set	XI to XIV									
Procedure	LSW	LSW	LSW	LSW	LSW	LSW	LSW	LSN	LSW	LSN
p	δ_2	δ_2	δ_2	2.1	1.6	2.0	δ_2	δ_{12}	2.1	1.7
σ	1.1E-6	2.7E-7	9.0E-7	1.7E-6	1.3E-7	8.3E-8	2.2E-8	3.1E-4	2.4E-11	1.6E-3
U_h (%)	4.0E-4	9.3E-5	1.1E-3	1.5E-3	4.8E-4	3.3E-5	2.5E-5	1.9E+1	5.8E-7	4.7E+2

Finally, it should be pointed out that the same procedure was applied to lower and higher AoAs, and the results were in the same orders of magnitude for all combinations of wings and methods. Therefore, Tabs. 3 and 4 accurately reflect the orders of magnitude of the uncertainties for the ranges of AoAs simulated in the Validation procedure.

3.1.2 Comparison with Results from Prandtl's Classic Lifting-Line Theory

To measure how much the methods deviate from the Classic Theory, the difference $\Delta C_L \equiv C_L - C_{L,CLL}$ between the results from numerical simulations and the analytic solution for elliptically-loaded wings, $C_{L,CLL}$, is assessed; $C_{L,CLL}$ can be written as[17,36]:

$$C_{L,CLL} = \pi AR \frac{1}{1 + \frac{4b}{\frac{\partial C_l}{\partial \alpha}\Big|_{y=0} c(0)}} \left[\alpha(0) + \theta(0)\right] \tag{21}$$

with AR the wing aspect ratio and b the wing span. Figure 5 shows ΔC_L versus α for fixed geometries, and versus AR, θ, and $\frac{\partial C_l}{\partial \alpha}$ for fixed α. In most cases, the α-method underestimated the magnitude of C_L while the Γ-method yielded the closest results to Prandtl's Theory, meaning the Γ-method is expected to overshoot experimental data. It remains to show that this is the case, which is one of the purposes of Validation.

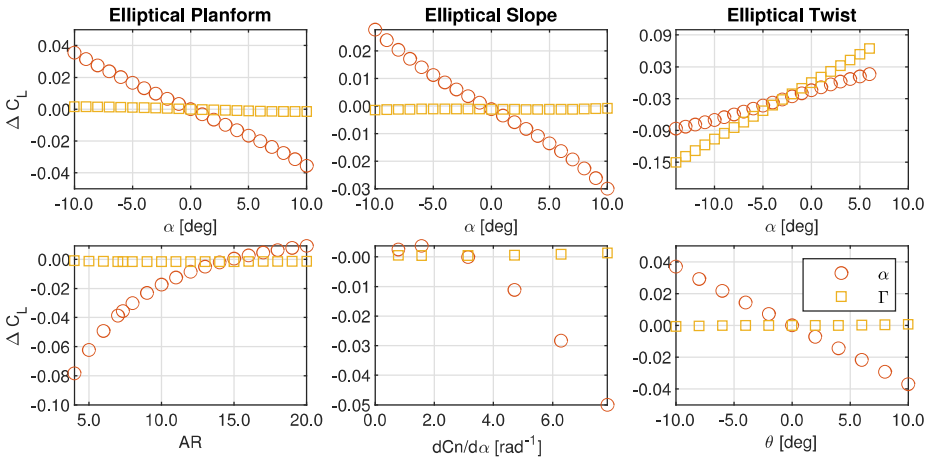

Figure 5. Difference between numerical and theoretical C_L versus α and some wing-design parameters for the α- and Γ-methods.

3.2 Validation

Both α- and Γ-methods are validated against experimental data and compared to numerical results reported in the literature; whenever possible, results followed these guidelines:

1. Airfoil data were the same for all methods, as they significantly impact the overall C_L and C_D. They generally came from the reference describing the numerical method(s) under comparison;
2. Uncertainties were combined through a standard uncertainty propagation so they would only be at the y-axis;
3. Numerical uncertainties considered all possible sources, such as grid, experimental inputs[15] (i.e., Re, α), and airfoil data. Whenever available, experimental uncertainties were also presented;
4. Cosine clustering was again used;
5. For wings with sweep or dihedral, results from the Γ-method were still presented, but with the uncertainties omitted for clarity. In these cases, the results should be rather assessed qualitatively.

3.2.1 *Almost-Elliptical Planform Wing*

Figures 6 and 7 present the results for the first wing, which has an elliptical planform with a rectangular inboard and NACA 0012 airfoil sections. Experiments[38] were performed at a free-stream Reynolds number $Re_\infty \approx 1.35 \times 10^6$ with respect to c_0. Along with the α- and Γ-methods, numerical results from an α-formulation (W-G) of Wickenheiser & Garcia[39] are also presented; but as the circulation distribution is cast as a sine series, the nonlinear scheme differs from the α-method as α_{eff} is directly updated. The 2-D airfoil data for all methods also comes from Wickenheiser & Garcia, which have been generated with JavaFoil using NACA standard surface finish and the Eppler standard transition model[39].

The $C_L \times \alpha$ plot on Fig. 6 shows that all numerical methods qualitatively agree with experiments up to stall, with the α-method performing suitably better at higher AoAs. From the $C_D \times \alpha$ plot, all methods overestimate the drag coefficient with respect to experiments by almost the same amount ΔC_D, which could have been addressed with more adequate source of airfoil data[31]. Additionally, in comparison to the α-method, the Γ-method slightly underpredicts C_D, specially at $5° \leq \alpha \leq 10°$.

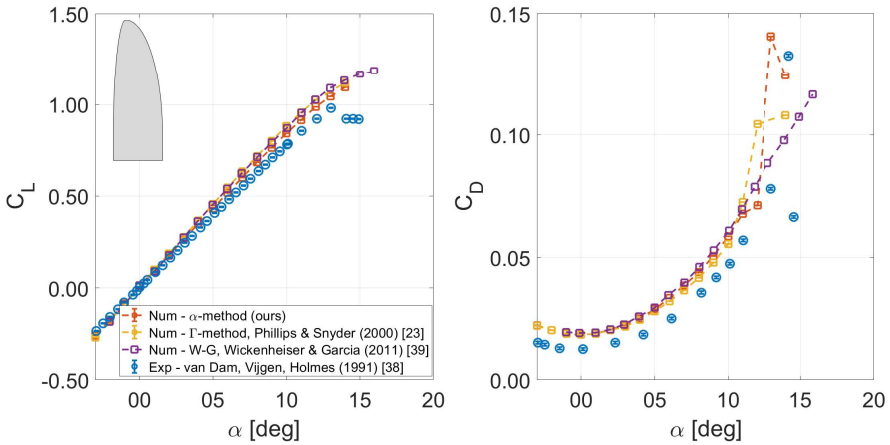

Figure 6. (left) $C_L \times \alpha$ and (right) $C_D \times \alpha$. Almost-elliptical planform wing.

In Fig. 7, the left plot presents $C_L \times C_D$ with the original data, while the right plot presents $C_L \times C_D$ with the numerical data corrected by ΔC_D so as to coincide with the experimental results; with this correction, it can be observed that the Γ-method tends to overpredict $\frac{L}{D}$, as expected from the previous discussion, while the W-G and α-method present similar $\frac{L}{D}$ values, close to the experimental data; as pointed out in the $C_L \times \alpha$ and $C_D \times \alpha$ plots, even though the differences in the W-G and α-methods are subtle, a similar $C_L \times C_D$ for these two methods is a consequence of the overprediction of both C_L and C_D for a given α in the case of the W-G method.

3.2.2 Crescent wing

The second wing has a similar planform but with a variable sweep angle distribution, and it has been experimented at the same conditions[38]. Numerical results from the W-G method are again shown for comparison, with the same source of 2-D data[39]. The results are illustrated in Fig. 8.

The $C_L \times \alpha$ plot shows that the overall agreement is again adequate, with all methods slightly overshooting the experimental data and both α- and Γ-methods performing slightly better. However, it is the presence of sweep that made the Γ-method perform similar to the α-, as well as to fail at higher AoAs, as previously indicated by the Verification procedure. Finally, no method adequately predicted stall, but the W-G seemed to predict the angle of occurrence.

For the $C_L \times C_D$ plot, the same right shift exists, but only the α-method kept a constant difference for most of the C_L range; so, as in the case of the almost-elliptical wing, in absence

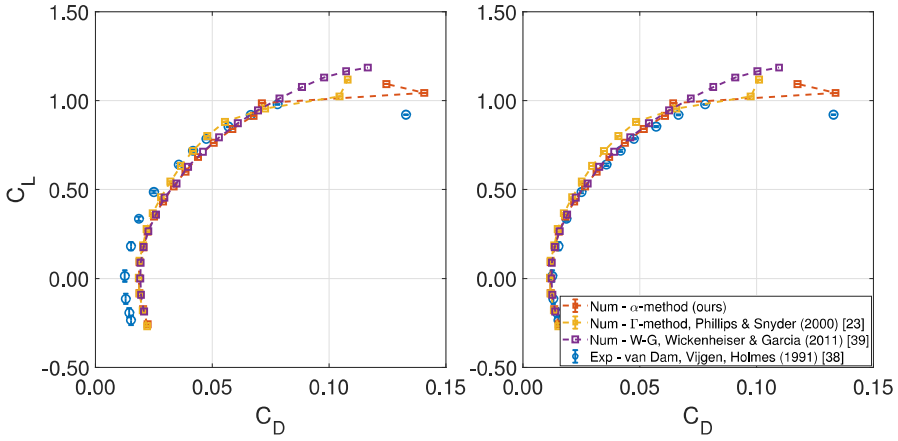

Figure 7. $C_L \times C_D$ (left) without and (right) with C_D shift. Almost-elliptical planform wing.

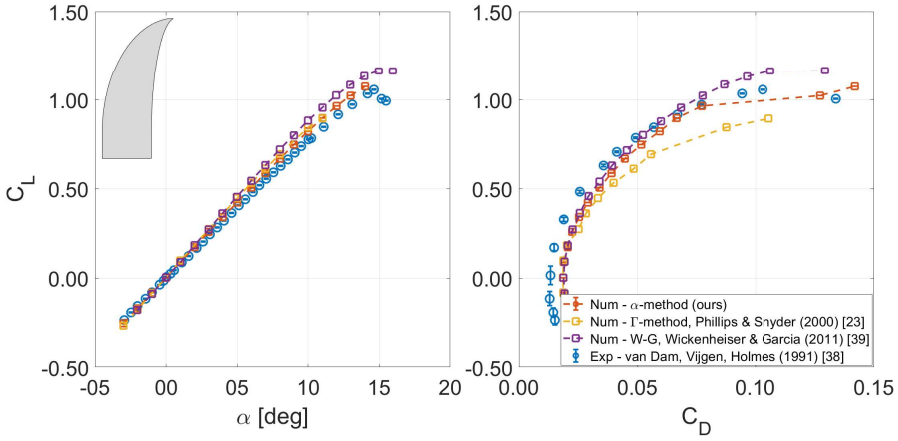

Figure 8. (left) $C_L \times \alpha$ and (right) . Crescent wing.

of such shift, W-G would overpredict efficiency, the Γ-method would underpredict it, and the α-method would yield the closest results to experiments.

3.2.3 Rectangular wing

Figure 9 shows the results for a NACA 0012 rectangular wing tested at $Re_\infty \approx 2.11 \times 10^6$ [40]. Numerical results from a mixed-formulation (WNLL) [22] and another Γ-formulation (PNLL) [24] are shown for comparison. The airfoil data used is from Owens [22], which assumes that $C_d = 0$, so a constant wing viscous drag contribution $C_{D0} = 0.009364$ was added to all α range.

The $C_L \times \alpha$ plot shows that, for most of the AoAs, the α-method and WNLL agree well to each other, and so the Γ-method and PNLL; the α-method and WNLL agree better to

the experimental data than the Γ-formulations, which present the C_L overshoot previously indicated in the Verification procedure. Additionally, for $\alpha \geqslant 12°$ the Γ-method presented convergence issues. Finally, the stall angle was correctly predicted only by the PNLL and WNLL.

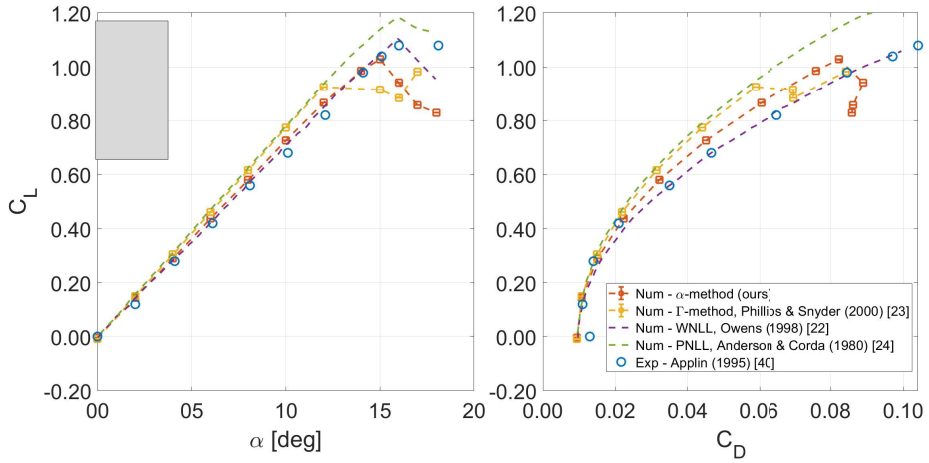

Figure 9. (left) $C_L \times \alpha$ and (right) $C_L \times C_D$. Rectangular wing.

The $C_L \times C_D$ curve shows that the Γ-formulations again overpredict $\frac{L}{D}$, while the best agreement happens for the WNLL, followed by the α-method. The differences between those two are nonetheless unexpected, as C_{Di} depends on C_L, which are similar for both, and since no different treatment for C_{Di} was reported in the implementation of WNLL[22], both formulations should yield similar curves.

3.2.4 45-deg Sweptback Wing

Results for a RAE-10112 45-deg sweptback wing are shown in Fig. 10, with experiments conducted at $Re_\infty \approx 1.68 \times 10^6$ [41] and numerical simulations from the WNLL[22] and an adaptation of the Γ-method (G-H)[33] that corrects it to enable the simulation of sweptback wings. The airfoil data was pre-generated by the open source code XFOIL[42] with its standard viscous model activated, while for the G-H method, a constant $\frac{\partial C_l}{\partial \alpha} = 5.935\ Rad^{-1}$ was assumed, while for the WNLL nothing has been reported.

From the $C_L \times \alpha$ curve, the differences between the Γ-method and its improved version (G-H) are readily observed; however, even with the G-H method addressing the convergence issues, it still does not address the lift overprediction of Γ-formulations, and again both the α-method and WNLL best match experimental data. The $C_L \times C_D$ plot corroborates the G-H $\frac{L}{D}$ overprediction while showing that the α-method best agrees with experimental data. For the WNLL, no results for C_D were reported[22].

Figure 11 shows the wing section lift distribution $C_{l,ws}$ at $\alpha = 4.2$ deg, normalized by C_L. As observed by Reid and Hunsaker[32], the Γ-method does not accurately predict $C_{l,ws}$, and the underpredicting lift that starts at root and propagates towards the tips is a direct consequence of the dependence of $\mathbf{V}$ on the grid resolution, as shown in the Verification section. In its improved version, the G-H method qualitatively agrees with the experimental data as well as

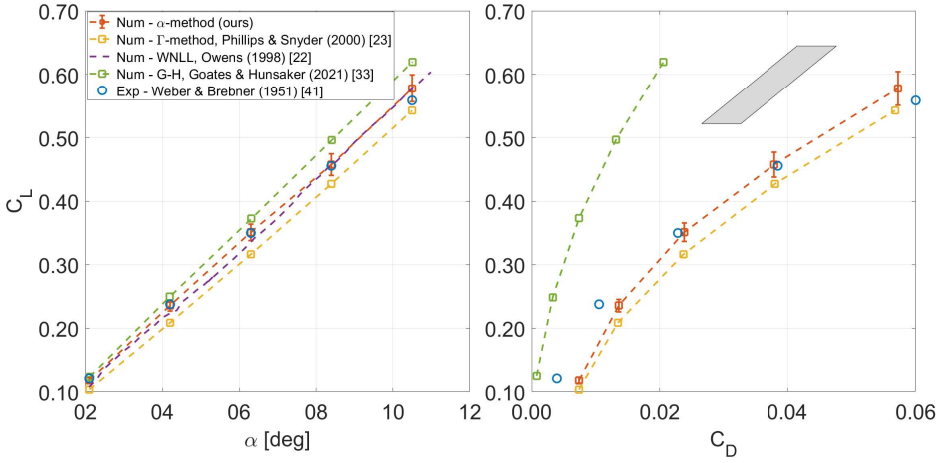

Figure 10. (left) $C_L \times \alpha$ and (right) $C_L \times C_D$. 45-deg sweptback wing.

the α-method.

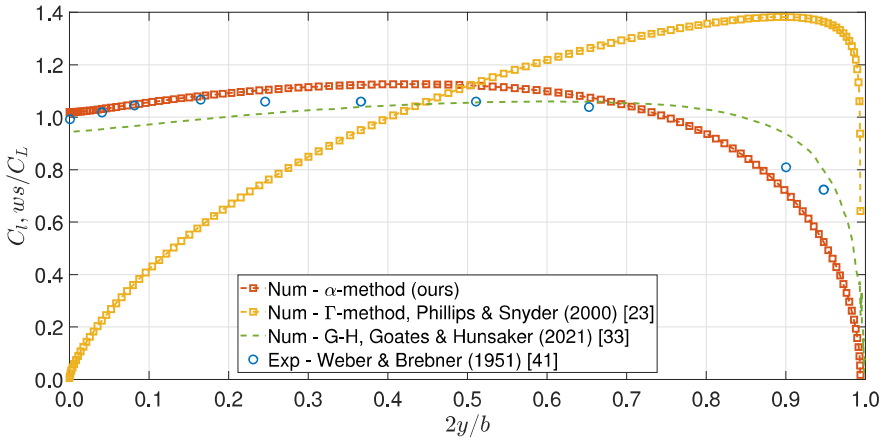

Figure 11. $\frac{C_{l_{ws}}}{C_L}$ distribution for $\alpha = 4.2°$. 45-deg sweptback wing.

3.2.5 *Twisted Wing with Taper*

The fifth wing has a linearly varying twist whose root and tip angles are $0°$ and $-3.50°$ and the respective airfoils are NACA 4420 and NACA 4412 with lofted sections in between. It also has a taper ratio $\frac{c(y=0)}{c(y=b)} = 2.5$ and a tip parabolic rounding[20], but the $\frac{c}{4}$ line is still straight. Experiments were conducted at $Re_\infty \approx 3.49 \times 10^6$ [43,20] (Wing '2.5-10-44,20'), which have also provided the source for airfoil data[20]. Figure 12 shows the results, which include the numerical simulations from the W-G α-formulation[39].

Both $C_L \times \alpha$ and $C_L \times C_D$ show that, up to stall, all methods compare well to experimental

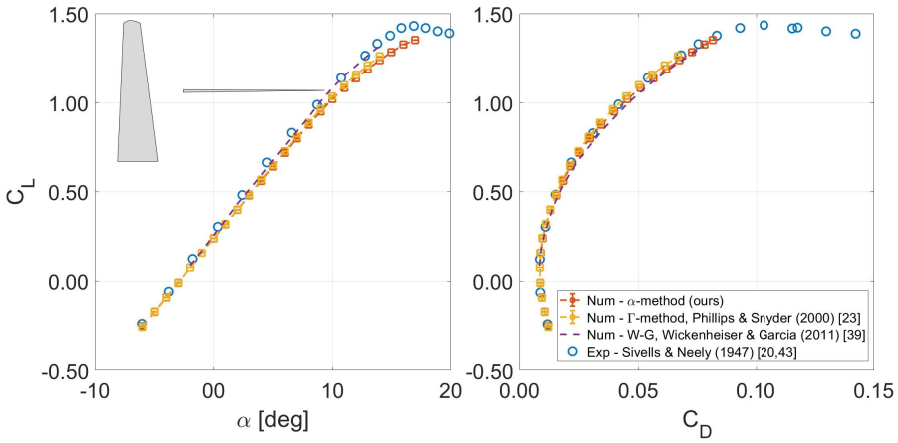

Figure 12. (left) $C_L \times \alpha$ and (right) $C_L \times C_D$. Twisted wing with 0.4 taper ratio.

data; while the polar plots look quite similar, the W-G[39] performed slightly better in the $C_L \times \alpha$ curve for higher AoAs, which could be a consequence of how the airfoil data in the mid-sections was calculated[31] (for both α- and Γ-methods it is done through linear interpolation, while for the W-G it is not reported), but further analysis would be necessary. Finally, the Γ-method failed to converge at higher AoAs.

3.2.6 3-deg Dihedral Wing with Taper

The last wing has a 3-deg dihedral, $\frac{c(y=0)}{c(y=b)} = 2.5$, tip parabolic rounding, and NACA 65210 sections throughout, whose data source comes from Abbott & Von Doenhoff[44,22,45]. Experiments were performed at $Re_\infty \approx 4.40 \times 10^6$ [45] and numerical simulations are again from the WNLL[22]. Figure 13 shows the results.

Both curves show that all numerical results compare well to experimental data, but the presence of dihedral prevented the Γ-method to converge for $\alpha \geqslant 8°$, as expected from the Verification procedure. Additionally, the α-method and the WNLL[22] present almost indistinguishable curves, which corroborates the discussion about the unexpected differences in the $C_L \times C_D$ plots observed for the straight wing case, Fig. 9.

4.0 Conclusion

This paper presented rigorous Verification & Validation procedures for two main Lifting-Line formulations that exist in the literature, named α- and Γ-methods. Verification, section 3.1.1, showed that the α-method converges well for all geometries with the highest grid uncertainty in the order of $10^{-3}\%$ and most convergence rates close to quadratic, while the Γ-method presented significantly larger uncertainties (in the order of $10^{+3}\%$) and low convergence rates for wings with dihedral and sweep, clearly pointing out convergence issues. Further comparison to analytic results from the Classic Formulation, section 3.1.2, revealed that the Γ-method agrees most with them, whereas the α-method typically yields lower absolute values, revealing a tendency of the Γ-method to overpredict C_L when compared to experiments. Validation, sec-

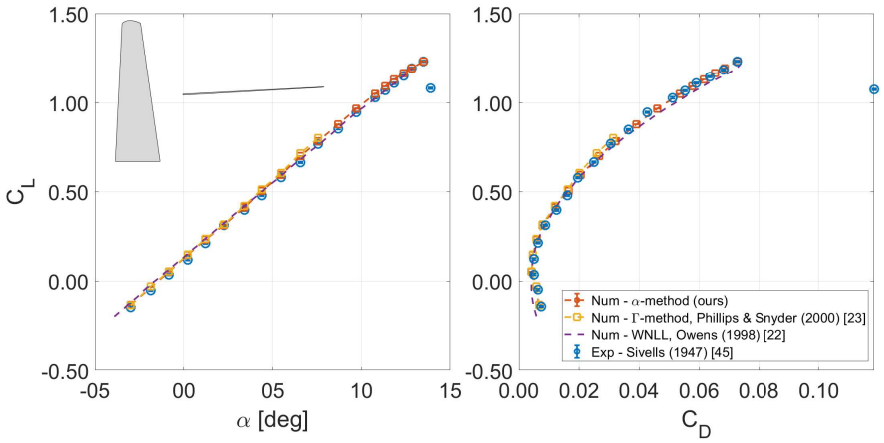

Figure 13. (left) $C_L \times \alpha$ and (right) $C_L \times C_D$. 3-deg dihedral wing with 0.4 taper ratio.

tion 3.2, corroborated the Γ-method convergence issues observed for wings with nonstraight $\frac{c}{4}$ lines and, even with modifications performed to circumvent them, its tendency to overpredict C_L. On the other hand, it showed that α-method is the one that best agreed with experimental data for most of the cases and, consequently, its advantages over the other methods presented.

As a final remark, in addition to the wake geometric construction and easy adaptation, the α-method capability of simulating wings of general geometry, confirmed by the V&V procedure, makes it potentially superior in the extension of modern Lifting Line methods to rotating lifting surfaces with nonstraight quarter-chord lines.

Acknowledgments

The authors acknowledge the financial support and scholarship granted by the Coordenação de Aperfeiçoamento de Pessoal de Nível Superior (CAPES), project 1655506, and the Fundação de Apoio ao Instituto de Pesquisas Tecnológicas (FIPT), notice 01/2016.

REFERENCES

1. Justin Winslow, Hikaru Otsuka, Bharath Govindarajan, and Inderjit Chopra. Basic understanding of airfoil characteristics at low reynolds numbers (104–105). *Journal of Aircraft*, 55(3):1050–1061, 2018. . URL https://doi.org/10.2514/1.C034415.
2. Elmiligui Alaa, Mohagna J. Pandya, Melissa B. Carter, Diskin Boris, and Sudheer N. Nayani. Usm3d simulations for the third aiaa sonic boom prediction workshop. *Journal of Aircraft*, 0(0):1–13, 2022. . URL https://doi.org/10.2514/1.C036429.
3. Richard Leloup, Kostia Roncin, Guilhem Bles, Jean-Baptiste Leroux, Christian Jochum, and Yves Parlier. Estimation of the lift-to-drag ratio using the lifting line method: Application to a leading edge inflatable kite. In *Airborne wind energy*, pages 339–355. Springer, 2013.

4. G Vernengo, L Bonfiglio, and S Brizzolara. Supercavitating three-dimensional hydrofoil analysis by viscous lifting-line approach. *AIAA Journal*, 55(12):4127–4141, 2017.
5. EmmanuelSimon Pierre Branlard. *Wind Turbine Aerodynamics and Vorticity-Based Methods: Fundamentals and Recent Applications*, volume 7 of *Research Topics in Wind Energy*. Springer, 2017. ISBN 978-3-319-55164-7. . URL `https://www.springer.com/gp/book/9783319551630`.
6. Jose Rodolfo Chreim, Marcos de Mattos Pimenta, Joao Lucas Dozzi Dantas, Gustavo RS Assi, and Eduardo Tadashi Katsuno. Development of a lifting-line-based method for preliminary propeller design. In *ASME 2018 37th International Conference on Ocean, Offshore and Arctic Engineering*, pages V002T08A008–V002T08A008. American Society of Mechanical Engineers, 2018. .
7. O Sugar-Gabor. A general numerical unsteady non-linear lifting line model for engineering aerodynamics studies. *The Aeronautical Journal*, 122(1254):1199–1228, 2018.
8. X Li, Z Zhou, and JH Guo. An unsteady aerodynamic model for three-dimensional wing based on augmented lifting-line method. *The Aeronautical Journal*, pages 1–19, 2022.
9. H Bertschneider, J Bosschers, GH Choi, E Ciappi, T Farabee, C Kawakita, and D Tang. Final report and recommendations to the 27th ittc. Technical report, International Towing Tank Conference, 2014.
10. A Sánchez-Caja, J Martio, I Saisto, and T Siikonen. On the enhancement of coupling potential flow models to rans solvers for the prediction of propeller effective wakes. *Journal of Marine Science and Technology*, 20(1):104–117, 2015.
11. WEIKANG DU, SPYROS A KINNAS, ROBIN MARTINS MENDES, and THOMAS LE QUERE. Rans/lifting line model interaction method for the design of ducted propellers and tidal turbines. In *Proceedings of the 22nd Offshore Symposium*, February 2017.
12. O. Şugar Gabor and A. Koreanschi. Fast and accurate quasi-3d aerodynamic methods for aircraft conceptual design studies. *The Aeronautical Journal*, 125(1286):593–617, 2021. .
13. L. Eca and M. Hoekstra. A procedure for the estimation of the numerical uncertainty of cfd calculations based on grid refinement studies. *Journal of Computational Physics*, 262:104 – 130, 2014. ISSN 0021-9991. . URL `http://www.sciencedirect.com/science/article/pii/S0021999114000278`.
14. Patrick J Roache. *Verification and validation in computational science and engineering*, volume 895. Hermosa Albuquerque, NM, 1998.
15. ASME. Standard for verification and validation in computational fluid dynamics and heat transfer. Standard, The American Society of Mechanical Engineers, New York, U.S.A, Mar 2009.
16. John David Anderson Jr. *Fundamentals of aerodynamics*. McGraw-Hill Education, 5 edition, 2010. ISBN 9780073398105.
17. Joseph Katz and Allen Plotkin. *Low-speed aerodynamics*, volume 13. Cambridge University Press, 2001.
18. J Weissinger. The lift distribution of swept-back wings. Technical report, NATIONAL ADVISORY COMMITEE FOR AERONAUTICS, 1947.

19. E Pistolesi. Considerations respecting the mutual influence of systems of airfoils. In *Collected Lectures of the 1937 Principal Meeting of the Lilienthal Society*, 1937.

20. James C Sivells and Robert H Neely. Method for calculating wing characteristics by lifting-line theory using nonlinear section life data. Technical Report 865, 1947.

21. Sylvain Gallay, Shahin Ghasemi, and Eric Laurendeau. Sweep effects on non-linear lifting line theory near stall. In *52nd Aerospace Science Meeting*, pages 2014–1105, 2014.

22. D Bruce Owens. Weissinger's model of the nonlinear lifting-line method for aircraft design. In *36th Aerospace Sciences Meeting and Exhibit AIAA Paper*, volume 597, 1998.

23. WF Phillips and DO Snyder. Modern adaptation of prandtl's classic lifting-line theory. *Journal of Aircraft*, 37(4):662–670, 2000.

24. John D. Anderson, Stephen Corda, and David M. Van Wie. Numerical lifting line theory applied to drooped leading-edge wings below and above stall. *Journal of Aircraft*, 17 (12):898–904, 1980. . URL https://doi.org/10.2514/3.44690.

25. José Rodolfo Chreim. *Development of a propeller Lifting-Line tool for analysis and design.* PhD thesis, Universidade de São Paulo, 2019.

26. C. P. van Dam, J. C. Vander Kam, and J. K. Paris. Design-oriented high-lift methodology for general aviation and civil transport aircraft. *Journal of Aircraft*, 38(6):1076–1084, 2001. . URL https://doi.org/10.2514/2.2875.

27. Marcos A Ortega, Roberto M Girardi, and Paulo S Komatsu. A numerical method to predict the lift of aircraft wings at stall conditions. In *10th Brazilian Congress of Thermal Engineering and Sciences*. ABCM - Associacao Brasileira de Engenharia e Ciencias Mecanicas, november-december 2004.

28. Sergio Luiz de Souza. Elaboração de uma metodologia para predição do coeficiente de sustentacao maximo de asas flapeadas. Master's thesis, Instituto de Tecnológico de Aeronáutica, 2005.

29. Douglas F Hunsaker. A numerical lifting-line method using horseshoe vortex sheets. Utah State University, 2011.

30. Jose Rodolfo Chreim. Extended lifting-line theory for viscous effects. Master's thesis, Universidade Federal do ABC, 2016.

31. Jose Rodolfo Chreim, Joao Lucas Dozzi Dantas, Karl Peter Burr, and Marcos de Mattos Pimenta. Viscous effects assessment through nonlinear lifting-line theory. In *24th ABCM International Congress of Mechanical Engineering*. ABCM - Associacao Brasileira de Engenharia e Ciencias Mecanicas, December 2017. .

32. Jackson T Reid and Douglas F Hunsaker. General approach to lifting-line theory, applied to wings with sweep. *Journal of Aircraft*, 58(2):334–346, 2021.

33. Cory D. Goates and Douglas F. Hunsaker. Practical implementation of a general numerical lifting-line method. In *AIAA Scitech 2021 Forum.* . URL https://arc.aiaa.org/doi/abs/10.2514/6.2021-0118.

34. Mark Drela. *Integrated simulation model for preliminary aerodynamic, structural, and control-law design of aircraft.* . URL https://arc.aiaa.org/doi/abs/10.2514/6.1999-1394.

35. Jose Rodolfo Chreim, Marcos Pimenta, Joao Lucas D Dantas, and Gustavo Assi. Changes in modern lifting-line methods for swept wings and viscous effects. In *2018 Applied Aerodynamics Conference*, page 3170, 2018. .

36. Brian J. Cantwell. Wings of finite span. https://web.stanford.edu/~cantwell/AA200_Course_Material/AA200_Course_Notes/AA200_Ch_12_Wings_of_Finite_Span_Cantwell.pdf, 2013.

37. A. R. Collar. On the accuracy of the representation of a lifting line by a finite set of horseshoe vortices. *Aeronautical Quarterly*, 9(3):232–250, 1958. .

38. C. P. van Dam, P. M. H. W. Vijgen, and B. J. Holmes. Experimental investigation on the effect of crescent planform on lift and drag. *Journal of Aircraft*, 28(11):713–720, 1991. . URL https://doi.org/10.2514/3.46087.

39. Adam M. Wickenheiser and Ephrahim Garcia. Extended nonlinear lifting-line method for aerodynamic modeling of reconfigurable aircraft. *Journal of Aircraft*, 48(5):1812–1817, 2011. . URL https://doi.org/10.2514/1.C031406.

40. Zachary T Applin. Pressure distributions from subsonic tests of a naca 0012 semispan wing model. Technical Memorandum 110148, National Aeronautics and Space Adminstration, Semptember 1995.

41. J Weber and GG Brebner. Low-speed tests on 45-deg swept-back wings. Technical Report 2882, 1951.

42. M Drela and H Youngren. Xfoil: An analysis and design system for low reynolds number airfoils. In *Low Reynolds Number Aerodynamics*. Springer, Springer, Berlin, Heidelberg, June 1989. ISBN 978-3-540-51884-6. .

43. Robert H Neely, Thomas V Bollech, Gertrude C Westrick, and Robert R Graham. Experimental and calculated characteristics of several naca 44-series wings with aspect ratios of 8, 10, and 12 and taper ratios of 2.5 and 3.5. Technical report, NATIONAL ADVISORY COMMITTEE FOR AERONAUTICS LANGLEY FIELD VA LANGLEY ..., 1947.

44. I.H. Abbott and A.E. Von Doenhoff. *Theory of Wing Sections, Including a Summary of Airfoil Data*. Dover Books on Aeronautical Engineering Series. Dover Publications, 1959. ISBN 9780486605869.

45. James C Sivells. Experimental and calculated characteristics of three wings of naca 64-210 and 65-210 airfoil sections with and without 2 deg washout. Technical report, NATIONAL AERONAUTICS AND SPACE ADMIN LANGLEY RESEARCH CENTER HAMPTON VA, 1947.